Quasi-Optical Slot Antenna SIS Mixers

Jonas Zmuidzinas, *Member, IEEE,* and H. G. LeDuc

Abstract—**We describe a new quasi-optical SIS mixer designed for efficient radiation coupling. The mixer uses a twin-slot antenna which has the advantages of a good beam pattern and a low impedance. The radiation and impedance characteristics of the antenna were obtained from a moment-method calculation. Tapered superconducting microstrip transmission lines are used to carry the radiation from the slot antennas to the tunnel junction. The effective impedance seen by the tunnel junction is quite low, about 4 Ω, which allows micron-size junctions to be used at 500 GHz. The mixers have been fabricated using Nb/Al-oxide/Nb tunnel junctions and a receiver noise temperature of 420 K (DSB) was measured at 490 GHz, which is the best yet obtained for a quasi-optical mixer at this frequency. The comparatively large junction area increases the mixer saturation power and allows strong suppression of noise from the Josephson effect by the application of a magnetic field of modest strength.**

I. Introduction

SUPERCONDUCTING tunnel junctions mixers (SIS mixers) are predicted to have sensitivities approaching the quantum limit well into the submillimeter wavelength band and perhaps to frequencies as high as twice the junction energy gap frequency [1]–[3]. However, the experimental realization of submillimeter SIS mixers has been difficult. There have been several reports in recent years (e.g. [4]–[6]) describing SIS mixers which directly couple the radiation from a free-space beam into a tunnel junction. These mixers use lenses to focus the radiation onto a microantenna which is fabricated lithographically along with the tunnel junction on the same substrate. Such quasi-optical designs avoid the problems associated with waveguides at short submillimeter wavelengths, and would make the fabrication of imaging mixer arrays a relatively straightforward task. However, previous quasi-optical mixers generally did not couple the radiation into the tunnel junction as efficiently as waveguide designs (e.g. [7]). The two critical factors in this coupling are the antenna efficiency—that is, how well the antenna pattern matches the incoming radiation, both in amplitude and phase—and the impedance match between the tunnel junction and the antenna. The slot antenna mixer design described in this paper is our first attempt at dealing with both of these issues in a design which is simple, robust, straightforward to fabricate, and relatively insensitive to fabrication tolerances.

Manuscript received October 1, 1991; revised January 29, 1992. This work was supported in part by NASA grant NAGW-107, NASA/JPL, an NSF Presidential Young Investigator grant to J. Zmuidzinas, and NSF grant DPP88-18384 (to University of Illinois).

J. Zmuidzinas is with the George W. Downs Laboratory of Physics, 320-47, California Institute of Technology, Pasadena, CA 91125.

H. G. LeDuc is with the Jet Propulsion Laboratory, 302-231, Pasadena, CA 91109.

IEEE Log Number 9201719.

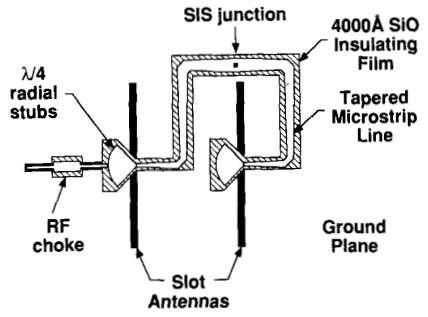

Fig. 1. A diagram of the slot-antenna mixer, showing the two slot antennas in a ground plane, the tapered microstrip line connecting each slot antenna to the SIS junction, the radial stubs which act as RF short circuits, and the RF choke for the dc bias and IF output.

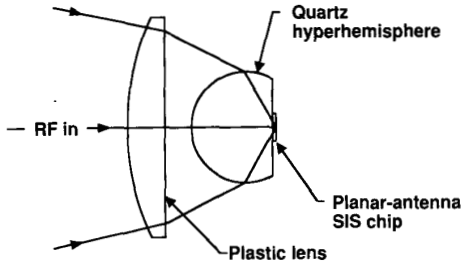

Fig. 2. The optical configuration of the twin-slot mixer, including the quartz hyperhemispherical lens and the plano-convex polyethylene lens.

Our mixer design consists of a twin-slot planar feed antenna, a planar Nb/Al-oxide/Nb SIS junction, and a tapered microstrip transmission line joining the junction to the two slot antennas (see Fig. 1). A hyperhemispherical lens is used to focus the incident radiation onto the twin-slot antenna (Fig. 2). A similar configuration for a 100 GHz quasi-optical Schottky mixer was described by Kerr, Siegel, and Mattauch [8]. The principal differences are that the Schottky design omitted the hyperhemispherical lens, used a quarter-wave section of transmission line for matching instead of a tapered line, was not monolithic (it used a whisker-contacted diode), and the two slots were fed in series instead of in parallel. A twin-slot antenna has also been used in a 94 GHz microbolometer, along with a layered dielectric stack in place of a hyperhemispherical lens [9].

II. Slot Antennas on Dielectric Substrates

The twin-slot antenna on a semi-infinite dielectric substrate has a number of desirable properties. The impedance is quite low, a highly symmetric pattern with a good efficiency can be obtained, and the polarization is linear. The antenna design was performed using a numerical moment-method analysis technique similar to that described by Kominami, Pozar, and Schaubert [10]. In the following, we give details of our particular implementation as well as our extensions to the method to allow two parallel slots to be computed including their interaction. The results of the analysis will then be presented along with the chosen design parameters.

A. Moment-Method Analysis

We define the z-axis to be normal to the antenna plane, and choose the x-axis along the slot. The length and width of the slot are L and W. Kominami, Pozar, and Schaubert derive an admittance kernel $Q(k_x, k_y)$ which relates the Fourier transforms of the y-components of the electric field and the surface current on the antenna plane, and is given by

$$Q(k_x, k_y) = \frac{1}{Z_0}\left[\frac{\epsilon_1 k^2 - k_x^2}{k\gamma_1} + \frac{\epsilon_2 k^2 - k_x^2}{k\gamma_2}\right]. \tag{1}$$

Here $Z_0 = 377\ \Omega$ is the impedance of free space, $k = \omega/c$ is the magnitude of the wave vector in free space, ϵ_1 and ϵ_2 are the dielectric constants above ($z > 0$) and below ($z < 0$) the antenna plane, and the z-component of the wave vector in the two half-spaces is $\gamma_\alpha^2 = \alpha k^2 - k_x^2 - k_y^2$, with the prescriptions Im $(\gamma_1) \le 0$ and Im $(\gamma_2) \ge 0$. The electric field in the slot is expanded in a set of basis functions $f_i(x, y)$:

$$E_y(x, y) = \sum_i V_i f_i(x, y), \tag{2}$$

which after Fourier transformation is multiplied by $Q(k_x, k_y)$ to yield the surface current J_y. Using the condition that the current must vanish inside the slot except at the feed point and using the basis functions f_i as testing functions (the Galerkin method) gives the usual matrix equation for the amplitudes V_i:

$$I_i = \sum_j Y_{ij} V_j. \tag{3}$$

The admittance matrix Y_{ij} is obtained from the admittance kernel and the Fourier transforms of the basis functions through numerical evaluation of integrals of the form

$$Y_{ij} = \frac{-1}{(2\pi)^2}\int_{-\infty}^{\infty}\int dk_x\, dk_y\, Q(k_x, k_y) f_i^*(k_x, k_y) f_j(k_x, k_y), \tag{4}$$

while the current moments I_i are each equal to the feed current I_f with a suitable normalization of the basis functions. We use the entire domain basis (EDB) functions given by Kominami, Pozar, and Schaubert [10], which prescribe a sinusoidal variation of the electric field in the slot. These functions are

$$f_i(x, y) = \frac{1}{\pi\sqrt{(W/2)^2 - y^2}} \cdot \begin{cases} \dfrac{\sin k_i(L/2 - |x|)}{\sin k_i L/2} & (i \text{ odd}) \\ \dfrac{1 - \cos k_i(L/2 - |x|)}{1 - \cos k_i L/2} & (i \text{ even}) \end{cases} \tag{5}$$

and we arbitrarily choose the parameters k_i to be roughly integer multiples of the propagation constant calculated using the mean dielectric constant $(1 + \epsilon_r)/2$; i.e., $1.6\,k$ for $i = 1, 2$; $3\,k$ for $i = 3, 4$; etc. Although the values k_i are in principle arbitrary, a judicious choice gives accurate results with fewer basis functions. Finally, the antenna impedance is obtained from the ratio of the voltage to current at the feed point:

$$Z_a = \frac{V_f}{I_f} = \sum_{ij} Z_{ij} \tag{6}$$

where the impedance matrix Z_{ij} is the inverse of the admittance matrix Y_{ij}. Equation (6) can be understood by recognizing that the voltage at the feed point ($x = 0$) is just the sum of the mode amplitudes V_i.

B. Calculation for a Twin-Slot Antenna

So far, we have discussed the case of a single slot antenna. Next, we consider two slots, labeled 1 and 2, with both slots parallel to the x-axis and centered at $(0, -S/2)$ and $(0, S/2)$ respectively, so that S is the separation of the slots. In this case, the overall admittance matrix is naturally partitioned into self-admittance and mutual-admittance blocks:

$$\boldsymbol{Y} = \begin{bmatrix} \boldsymbol{Y}^{11} & \boldsymbol{Y}^{12} \\ \boldsymbol{Y}^{21} & \boldsymbol{Y}^{22} \end{bmatrix}. \tag{7}$$

The self-admittance matrix elements $Y_{ij}^{11} = Y_{ij}^{22}$ for each slot are computed exactly as before in the single-slot case, while the mutual-admittance matrix elements are given by

$$Y_{ij}^{12} = Y_{ij}^{21} = \frac{-1}{(2\pi)^2}\int_{-\infty}^{\infty}\int dk_x\, dk_y\, Q(k_x, k_y) \cdot f_i(k_x, k_y) f_j(k_x, k_y) \cos k_y S. \tag{8}$$

Here we have suppressed the complex conjugate on f_i since the Fourier transforms of our basis functions are purely real. Inverting the admittance matrix $\boldsymbol{Y}$ gives the impedance matrix $\boldsymbol{Z}$, which is then partitioned:

$$\boldsymbol{Z} = \begin{bmatrix} \boldsymbol{Z}^{11} & \boldsymbol{Z}^{12} \\ \boldsymbol{Z}^{21} & \boldsymbol{Z}^{22} \end{bmatrix}. \tag{9}$$

Of course, $\boldsymbol{Z}^{11} = \boldsymbol{Z}^{22}$ and $\boldsymbol{Z}^{12} = \boldsymbol{Z}^{21}$ by symmetry. The twin-slot antenna can be considered as a passive two-port network, with the feed point of each slot serving as a port.

the corresponding two-port impedance matrix is

$$\mathbf{Z}_{\text{two-port}} = \begin{bmatrix} \sum_{ij} Z_{ij}^{11} & \sum_{ij} Z_{ij}^{12} \\ \sum_{ij} Z_{ij}^{21} & \sum_{ij} Z_{ij}^{22} \end{bmatrix} \tag{10}$$

so in the case of symmetric excitation, the impedance of each slot antenna is

$$Z_a = \sum_{ij} (Z_{ij}^{11} + Z_{ij}^{12}). \tag{11}$$

C. Radiation Pattern

The moment-method also allows the antenna patterns to be calculated from the electric field in the slots. First, the mode amplitudes V_i can be calculated from the impedance matrix using

$$V_i = I_f \sum_j (Z_{ij}^{11} + Z_{ij}^{12}). \tag{12}$$

The mode amplitudes V_i allow the electric field in the slots to be calculated in the Fourier domain:

$$E_y(k_x, k_y) = \sum_i V_i f_i(k_x, k_y). \tag{13}$$

Finally, the radiated electric field is given in polar coordinates (r, θ, ϕ) by

$$\boldsymbol{E}_\alpha(r, \theta, \phi) = \frac{\exp(-ik_\alpha r)}{r} \boldsymbol{g}_\alpha(\theta, \phi) \tag{14}$$

where the amplitude and polarization of the electric field radiated in the direction (θ, ϕ) is obtained from $E_y(k_x, k_x)$ using:

$$\begin{aligned} \boldsymbol{g}_\alpha(\theta, \phi) = {} & \frac{-ik_\alpha}{\pi} E_y(k_\alpha \sin\theta \cos\phi, k_\alpha \sin\theta \sin\phi) \\ & \times \cos\left(k_\alpha \frac{S}{2} \sin\theta \sin\phi\right) \\ & \cdot [\cos\theta\, \hat{y} - \sin\theta \sin\phi\, \hat{z}]. \end{aligned} \tag{15}$$

Here $\alpha = 1, 2$ labels the half-space $z > 0$ or $z < 0$ (or equivalently, $0 \le \theta < \pi/2$ and $\pi/2 < \theta \le \pi$) and $k_\alpha = \epsilon_\alpha^{1/2} k$. The factor $\cos(k_\alpha [S/2] \sin\theta \sin\phi)$ is simply the array factor for two antennas separated by a distance S along the y-axis. The power dP radiated into a solid angle $d\Omega$ is given by

$$\frac{dP}{d\Omega} = \frac{\sqrt{\epsilon_\alpha}}{Z_0} |\boldsymbol{g}_\alpha(\theta, \phi)|^2, \tag{16}$$

as can easily be seen by calculating the Poynting vector $\boldsymbol{S} = \boldsymbol{E} \times \boldsymbol{H}$ and using $|\boldsymbol{H}| = \epsilon_\alpha^{1/2} |\boldsymbol{E}| / Z_0$.

D. Results—Antenna Impedance

We have developed a program to perform this analysis. We checked our program by repeating the calculations of Kominami *et al.* [10] and obtained identical results. However, Kominami *et al.* presented calculations for Teflon ($\epsilon_r = 2.55$) and GaAs ($\epsilon_r = 12.8$) substrates but not for crystal quartz ($\epsilon_r = 4.53$). The impedance as a function of frequency we calculate for a single slot in the case of a crystal quartz substrate is shown in Fig. 3. Two basis functions were used in the computation. Including more basis functions did not substantially affect the results, and Kominami *et al.* demonstrated good agreement between calculations done using two extended-domain basis functions (EDB) and five piecewise sinusoidal basis functions (PWS). In the calculation we have ignored the fact that quartz is slightly birefringent and have assumed $\epsilon_r = 4.53$ [11], which is an average of the dielectric constants for the ordinary and extraordinary rays. Since these two dielectric constants differ by only about 4.5%, the error in the calculated impedance incurred by treating quartz as an isotropic material will be less than $\pm 1\%$. Note also that the values of the dielectric constants at room temperature and at 4 K differ by no more than 1% [12]. Fig. 3 shows that the slot antenna has a broad region of low impedance which lies in between two high-impedance resonances. The impedance of a single slot antenna of length $L = 0.47\ \lambda$ (where λ is the free-space wavelength) and width $W/L = 0.04$ is $Z_a = 35 + j0\ \Omega$. The antenna impedance bandwidth is quite broad. The frequency band over which the fractional power coupled from the antenna into a 35 Ω load is better than 50% is one octave. The main effect of the mutual interaction of two symmetrically-fed slots separated by $S = 0.3\ \lambda$ is that the length at which the antenna impedance becomes purely real increases slightly, by about 8%.

The behavior of the impedance of a slot antenna can be understood intuitively by considering a slot antenna as two short-circuited lossy slot transmission lines in parallel. For a given substrate, the amount of (radiative) loss is controlled by the ratio of the slot width W to the wavelength λ. The high-impedance resonances arise when the total length of the slot antenna is an odd multiple of $\lambda_g/2$, where λ_g is the propagation wavelength on the slot line, and is approximately $\lambda_g \approx [\lambda/\sqrt{(\epsilon_1 + \epsilon_2)/2}]$. Apart from the resonances, the impedance of a slot antenna is low. Unfortunately, treating the antenna as a slot transmission line does not give an accurate estimate of the "antiresonant" frequencies. The behavior of a slot antenna is complementary to that of a metal strip dipole antenna, which has narrow-band low impedance resonances and broad high impedance regions. A slot antenna is therefore much better suited than a dipole to matching low impedance devices over broad bandwidths.

E. Results—Antenna Pattern

A contour plot of the power pattern radiated into the dielectric is shown in Fig. 4. The contours are linearly spaced, from 5% to 95% of the peak in increments of 5%. This pattern was calculated using the results of the moment-method analysis including the mutual interaction between the slots. The separation between the slots ($S = 0.29\ \lambda$) was adjusted to produce a symmetric pattern with a half-power beam width of 47°. The main beam effi-

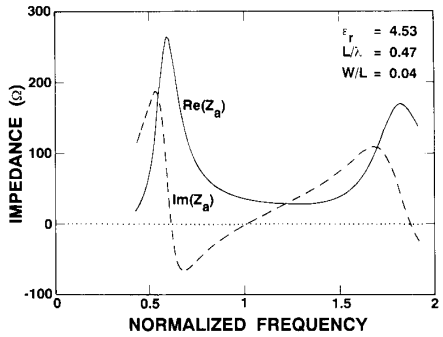

Fig. 3. The impedance as a function of frequency calculated for a single slot antenna on a semi-infinite dielectric substrate. The slot length is $L = 0.47\ \lambda$, the width is $W = 0.04\ L$, and the dielectric constant of the substrate is $\epsilon_r = 4.53$.

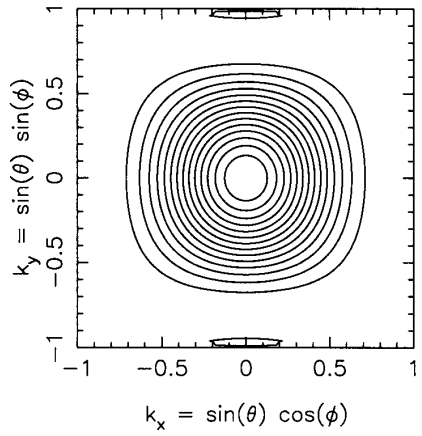

Fig. 4. A contour plot of the calculated power pattern radiated into the dielectric by the twin-slot antenna. The dimensions of the slots are the same as in Fig. 3, and the separation of the slots is $S = 0.29\ \lambda$. The contours are linearly spaced from 5% to 95% of the peak power, in increments of 5%.

ciency is calculated to be $\eta_{MB} = 70\%$. The remaining power is radiated into small E-plane sidelobes (4%) and backwards into air (26%). The E-plane sidelobes are grating lobes for the two-slot array. The power in these sidelobes can be reduced by placing the slots closer together, at the expense of some degradation of the beam symmetry. The power division ratio is about 2.8 : 1 in favor of the dielectric, which is much closer to the ratio of $\epsilon_r^{1/2} \approx 2.1$ expected for a narrow-beam antenna on a dielectric substrate than to the ratio of $\epsilon_r^{3/2} \approx 9.6$ predicted for a very broad-beam radiator [13].

The phase of the antenna pattern was also investigated. The antenna does have a small phase error, but fortunately this error causes a reduction in the coupling efficiency of less than 2%. This error is due to a slight astigmatism: the E-plane and H-plane phase centers are slightly displaced from each other in a direction normal to the substrate. The twin-slot antenna has excellent polarization characteristics since it responds only to electric fields perpendicular to the slots. The cross-polarization response of the *mixer* is largely determined by the hyperhemispherical lens, because the transmission through the air/dielectric interface at the lens surface depends on the polarization and angle of incidence. We have not calculated this effect, but do not expect it to reduce the coupling efficiency to a linearly polarized beam substantially.

III. Mixer Optics

Two lenses are used in the mixer, a crystal quartz hyperhemispherical lens and a plano-convex high-density polyethylene lens (Fig. 1). The hyperhemisphere has a diameter of 0.500 in., and the height is chosen so that the mixer chip is at the aberration-free focus located at a distance of R/n from the center of the spherical surface, where R is the radius of the lens and n is the index of refraction. The quartz hyperhemispherical lens transforms the fairly broad beam of the twin-slot antenna (HPBW = 47°) to a narrower beam (HPBW = 22°), and it prevents power from being radiated into surface-wave modes as occurs when finite-thickness dielectric substrates are used. However, there is a reflection loss associated with the air-dielectric interface of the lens, which we calculate to be about 14% averaged over the antenna beam. This loss can be almost completely eliminated by using a quarter-wave anti-reflection coating. The plastic lens serves to convert the 22° HPBW beam exiting the hyperhemisphere into a narrower beam that matches well to a telescope.

Aberrations in the focusing lenses can arise from imperfect dimensions or positioning of the lenses, or may be intrinsic to the lens design (as is the case for our plastic lens). To evaluate these effects, a program was written to calculate the coupling efficiency of the lens system within the framework of ray optics, which should be valid since the diameter of our hyperhemisphere is about 20 wavelengths at 500 GHz. The ray trace is used to construct the wavefront of the aberrated beam, using the principle that the rays are normal to the wavefront [14]. The phase error Φ of the aberrated wavefront as compared to a perfect spherical wavefront centered on the nominal focus is given by

$$\Phi(\theta) = \frac{2\pi n}{\lambda} \int_0^{\theta} d\theta'\ \delta(\theta')\ \cos(\theta') \qquad (17)$$

where $\delta(\theta)$ is the distance in the antenna plane from the optical axis to the aberrated ray at incidence angle θ. This phase error is used in calculating the coupling efficiency between the incoming beam and the antenna pattern. The calculation indicates that spherical aberration in the plastic lens reduces the coupling efficiency by less than 2%. The most critical dimension in the optics is the height of the hyperhemisphere: at 500 GHz, an error of ±0.005 in. results in a 10% reduction of the coupling efficiency. The calculation also shows that the birefringence of quartz should not be a problem. The heights of the hyperhemisphere calculated using the ordinary or extraordinary ray refractive indexes differ by only $\Delta h = R/n_o - R/n_e = 0.0026$ in., well within the ±0.005 in. tolerance.

IV. Transmission Lines

To match the 35 Ω twin-slot antenna impedance to the SIS junction we use two superconducting microstrip transmission lines. These lines are tapered from a characteristic impedance of 35 Ω at each slot to an impedance of 8 Ω at the junction. Since the two transmission lines feed the junction in parallel, the impedance seen by the junction is 4 Ω. The ground plane of the slot antenna is used as the ground plane for the microstrip transmission line. The presence of the ground plane simplifies the design of the antenna feed lines and minimizes interactions between the feed lines and the incident radiation.

The characteristic impedance, phase velocity, and loss of the superconducting microstrip transmission lines used in the design of the mixer were calculated in the manner described by Whitaker *et al.* [15] and Kautz [16]. First, the behavior of a transmission line made from a perfect conductor ($\sigma = \infty$) is calculated, which gives the series impedance Z and the shunt admittance Y per unit length of line. In order to include the effects of fringing fields and dispersion we use the design equations for microstrip given by Hammerstad and Jensen [17] to calculate Z and Y, instead of the simple parallel plate approximation used by Kautz. Once Z and Y are obtained, the effect of replacing the perfect conductor by a superconductor is approximated by introducing an extra contribution to the series impedance of the line: $Z' = Z + gZ_s$, where Z_s is the surface impedance of the superconductor and g is a geometrical factor. The propagation constant and characteristic impedance of the superconducting line can then be calculated using the modified series impedance Z' and the original shunt admittance. The geometrical factor for microstrip is calculated from $g = 2K/w$, where the correction factor K is approximately given by

$$K = \exp\left[-1.2\left(\frac{Z_{01}}{\eta_0}\right)^{0.7}\right] \tag{18}$$

in the notation of Hammerstad and Jensen [17]. The surface impedance Z_s is calculated using expressions [15], [16] for the case of local electrodynamics for the superconductor. We have compared the surface impedance of Nb calculated in this local approximation to that calculated using the full nonlocal Mattis-Bardeen theory [18]–[20], and find that the real part of the surface impedance calculated in the local approximation is less than that predicted by the nonlocal theory by about 20–30% in the range 100–800 GHz. Thus, a calculation which assumes local electrodynamics may somewhat underestimate the loss of superconducting Nb microstrip lines, but this should not be important since the predicted loss at 500 GHz is quite low, about 1% per propagation wavelength at 4.2 K.

Despite our efforts to calculate the parameters of superconducting microstrip lines carefully, our capability of predicting the behavior of real transmission lines is hindered by our lack of accurate knowledge of the properties of our superconducting (Nb) and insulating (SiO) films. Thus, we chose to use a tapered transformer between the junction and the slot antennas, since a taper is less sensitive to the exact values of characteristic impedance and phase velocity. The characteristic impedance of the line is tapered from $Z_1 = 35$ Ω at the slot antenna to $Z_2 = 8$ Ω at the junction. The impedance as a function of position x on a line of length L was chosen to be

$$Z(x) = Z_1 \exp\left\{\frac{1}{2}\ln\left(\frac{Z_2}{Z_1}\right)\left[\sin\left(\pi\left(\frac{x}{L} - \frac{1}{2}\right)\right) + 1\right]\right\} \tag{19}$$

as suggested by McGinnis and Beyer [21] for good broadband performance. Typical dimensions are $w = 2$ μm at the slot antenna, $w = 12$ μm at the junction, and $s \approx 5000$ Å for the thickness of the SiO dielectric. The overall length of the tapered line from each slot antenna to the junction is about 2 propagation wavelengths.

The coupling between the microstrip and the slot antenna is achieved by using a radial transmission-line stub, which is a good broad-band RF short circuit [22] but an open circuit at dc. At RF, the radial stub short-circuits the microstrip line to one side of the slot antenna. The RF current must then flow around the edges of slot antenna and return on the portion of the ground plane directly underneath the microstrip. An RF choke circuit is attached to the end of the radial stub to allow dc bias to be brought in and the IF to be coupled out.

V. Impedance Matching

As compared to other submillimeter mixer designs, our slot-antenna mixer uses an SIS junction with a fairly large area. Larger area junctions have a higher saturation power, require a smaller magnetic field to suppress the Josephson effect, are easier to fabricate, and are electrically more robust. The disadvantages of using larger junctions are that such junctions require more LO power and have a lower impedance which is more difficult to match. At high frequencies, the reactance of the junction capacitance is much lower than the normal-state resistance of the junction, and so the magnitude of the complex impedance of the junction is $|Z| \approx 1/\omega C$ to a good approximation. Our mixer design does not attempt to tune out the junction capacitance with an inductive shunt or a microstrip stub. Rather, we transform the antenna impedance down to a level of $1/\omega C$, which gives the best possible match to the junction under the constraint of a purely real source impedance. We have intentionally avoided using resonant circuits in our initial design, because such circuits have tighter dimensional tolerances and require good knowledge of the behavior of superconducting transmission lines at high frequencies.

In our circuit, the optimum junction area scales inversely with frequency and is ≈ 1 μm^2 at 500 GHz; our design rule is that $1/\omega C = 4$ Ω. We have arbitrarily chosen this impedance to be 4 Ω, simply because this was about the highest impedance which would still allow the use of a junction manufactured with optical lithography—

at 500 GHz, $1/\omega C \approx 4\ \Omega$ for a high current density ($J_c = 10$ kA cm^{-2}) Nb/Al-oxide/Nb junction when the junction area is 1 μm^2. Here we have assumed a specific capacitance of $C_s = 80$ fF μm^{-2} [23], a value now believed to be appropriate for Nb/Al-Oxide/Nb junctions with $J_c = 10$ kA cm^{-2}. Unfortunately, the mixers were designed assuming a specific capacitance of $C_s = 50$ fF μm^{-2} measured for $J_c \approx$ 1–3 kA cm^{-2} [24], [25], which gives areas of 1.5 μm^2 at 500 GHz. The actual junction areas are about 2.3 μm^2 because the mask design overcompensated for possible shrinkage in the junction dimensions during manufacture. We have made a sacrifice in the coupling efficiency by not attempting to tune out the junction capacitance. The impedance coupling efficiency for a 1 μm^2 junction would be about 32%, but is reduced to around 23% in our present devices because the junction area (≈ 2.3 μm^2) is larger than optimum.

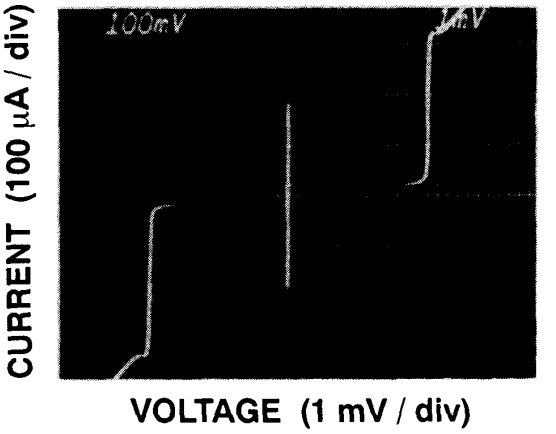

Fig. 5. The I–V curve of a Nb/Al-Oxide/Nb tunnel junction in a slot-antenna mixer circuit. The junction has an area of 2.3 μm^2, a critical current density of 10 kA cm^{-2}, and a normal-state resistance of 9 Ω.

VI. Device Fabrication

The twin-slot mixers were fabricated at the Microdevices Laboratory at JPL, using a four mask level Nb/Al-Oxide/Nb fabrication process similar to the planar NbN/MgO/NbN process described by LeDuc *et al.* [26]. The devices were fabricated on 1 in. square, 10 mil thick crystal quartz substrates using only optical lithography. Thermally evaporated SiO is used as the dielectric for the superconducting microstrip line. The required thickness of 4000–5000 Å is obtained in two steps: a 1500 Å thick layer deposited during the junction isolation step, and a second layer about 2500 to 3500 Å thick evaporated through a photoresist lift-off stencil. The fabrication results were quite good. The SIS junctions tested at 500 GHz had areas of $A \approx 2.3$ μm^2, normal-state resistances of $R_N = 9\ \Omega$, current densities of $J_C \approx 10$ kA cm^{-2}, and $\omega R_N C \approx 5.3$. A typical I–V curve is shown in Fig. 5. The yield was high: 36 out of 37 devices tested had good I–V curves (i.e. similar to Fig. 5). The rms variation in the current step at the gap voltage was 4.5%, and the typical normal to subgap resistance ratio was $R_{sg}/R_N \approx 10$.

VII. Mixer Assembly

Three crystal quartz pieces actually make up the hyperhemispherical lens: a 0.500 in. diameter hyperhemisphere whose height is 0.050 in. shorter than required for proper focusing; a 1 in. diameter, 40 mil thick disk; and the SIS chip, whose dimensions are typically 40 × 60 × 10 mils. The disk is clamped in place in the mixer block which is machined from OFHC copper. Indium foil is placed in between the disk and the block to assure good thermal contact and to minimize breakage. The hyperhemisphere and the SIS chip are glued to opposite sides of the disk using a UV-curing glue [27]. The UV-curing glue allows the SIS chip and hyperhemisphere to be easily positioned under a microscope with respect to alignment marks on the disk; once they are in the proper position, an ultraviolet lamp is turned on which exposes and sets the glue. A 25 Ω microstrip line fabricated on 10 mil crystal quartz is also glued onto the disk and serves to carry the IF from the SIS chip at the center of the disk to the edge of the disk, where it is then connected to a microwave circuit board containing the IF matching network. The electrical connections between the SIS chip and quartz microstrip are made with 1 mil dia. aluminum wire using an ultrasonic wedge bonder. The quartz microstrip is slightly oversized near the SIS chip; this provides ≈ 0.5 pF additional capacitance which helps to short-circuit the SIS chip at higher out-of-band IF frequencies [28]. The IF matching network consists of a single quarter-wave section which matches the $\approx 25\ \Omega$ dynamic resistance of the pumped SIS I-V curve to 50 Ω over the 1.25–1.75 GHz IF bandwidth. The mixer block is mounted directly on the 4.2 K cold plate of a liquid helium dewar [29], as is the 1.25–1.75 GHz HEMT IF amplifier [30]. The radiation enters the dewar through a 1 mil thick mylar vacuum window. Room-temperature infrared radiation entering the dewar through the vacuum window is filtered out by a crystal quartz disk which is anti-reflection coated with black polyethylene and is mounted on a radiation shield cooled to 77 K. Additional filtering is provided by a 15 mil thick Fluorogold sheet, mounted directly on the mixer block in front of the plastic lens.

VIII. Test Results

Initial laboratory tests of the slot-antenna mixer have been very encouraging. The 490 GHz local oscillator was a 98 GHz InP Gunn oscillator [31] followed by a Schottky varactor quintupler [32]. The local oscillator was introduced into the signal path by using a 12% reflective mylar beamsplitter. With this arrangement, the mixer could be pumped with substantially more than the minimum LO power necessary for efficient mixing. The receiver sensitivity was measured with the standard hot/cold load Y-factor technique, using sheets of Eccosorb at room temperature (295 K) and dipped in liquid nitrogen (80 K).

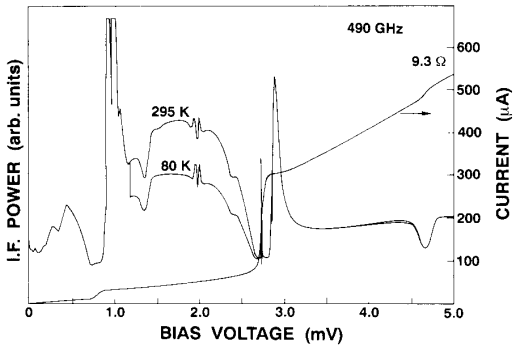

Fig. 6. Results of heterodyne measurements of the receiver sensitivity at 490 GHz. Shown is the IF power as a function of bias voltage for hot (295 K) and cold (80 K) loads placed into the receiver beam. Also shown is the pumped I-V curve with photon-assisted tunneling step widths of $h\nu/e \approx 2$ mV. Although no structure is visible in the I-V curve near the expected locations of the Shapiro steps (1 mV, 2 mV, etc.) due to the applied magnetic field, features are visible in the IF power curves at these voltages.

The IF noise temperature and gain were calibrated by biasing the SIS junction above the gap voltage and using the shot noise produced by the junction as a variable temperature IF load [33]. The measured IF power for the hot and cold loads as a function of voltage is shown in Fig. 6. These data were obtained by suppressing the Josephson effect with a magnetic field. Structure is still visible in Fig. 6 in the vicinity of the second Shapiro step at 2 mV, but is suppressed to a remarkable degree compared to the case with no magnetic field. The application of the magnetic field allows low-noise mixing over a large fraction of the first photon step below the gap voltage. Without the field applied, reliable mixer operation could not be obtained. The receiver noise temperature was measured to be 420 K (DSB). The shot-noise calibration of the IF allowed the conversion loss to be estimated at approximately 10 dB (DSB). The contribution of the IF system to the receiver noise is about 110 K, while the beamsplitter adds 70 K. Subtracting these contributions gives an upper limit to the *mixer* noise temperature of about 240 K (DSB). Because the mixer should be broad-band, we expect the two sidebands of the mixer to have equal response.

Possible non-heterodyne response of the mixer was investigated by performing hot/cold load measurements with the local oscillator turned off. We detected very small changes in the IF output power of the mixer when the cold load was substituted in place of the hot load with the LO turned off, but this response was strongly dependent on the bias voltage. The variation of the mixer IF power was weaker with the LO turned off than with the LO turned on by factors of 100, 30, and 11, for bias voltages of 1.75, 2.18, and 2.50 mV, respectively. The noise temperatures measured at these bias voltages (with the LO on) were fairly constant, about 490, 420, and 460 K, respectively. Although these tests are not absolutely conclusive, they do give strong evidence that with the LO on we are measuring predominantly heterodyne response.

TABLE I
ESTIMATED CONTRIBUTIONS TO MIXER CONVERSION LOSS (SSB)

Contribution	Loss (dB)
Plastic lens (reflection loss)	0.41
Hyperhemisphere (reflection loss)	0.66
Other optical effects (aberrations, birefringence, cross-polarization, SIS chip positioning errors, antenna phase error)	0.50
Antenna efficiency	1.55
Microstrip line attenuation	0.10
Intrinsic junction conversion loss	10–12
Overall conversion loss:	13.2–15.2

Further evidence that this is the case is given by the shape of the IF power versus bias voltage curves (Fig. 6), which show good response over most of the first photon step. We have not yet determined why the direct-detection response with the LO turned off becomes stronger as the bias voltage is increased, although there are several possible explanations including mechanisms involving direct detection by photon-assisted tunneling or radiative heating of the tunnel junction.

IX. DISCUSSION AND CONCLUSIONS

One of the most interesting results is the degree to which the magnetic field suppresses noise from the Josephson effect (Fig. 6). These results give us confidence that low-noise SIS mixing should be possible up to at least the gap frequency (700 GHz for Nb; $\approx$1400 GHz for NbN), and confirms previous experience with Pb-alloy SIS mixers at 500 GHz [34]. Excess noise produced by the Josephson effect has been thought to be a major limiting factor in the performance of SIS mixers at high frequencies [1], [35]. While it is well known that a magnetic field applied to a junction can almost completely suppress the dc Josephson current, it has not been clear that high-frequency noise currents would also be suppressed to a similar extent. Our results agree with the conclusions of Winkler and Claeson [36], who studied SIS and SIN mixing in Al tunnel junctions at frequencies ($\approx$75 GHz) approaching the superconducting gap frequency of Al ($\approx$90 GHz).

There is considerable room for improvement of the present mixer. Table I gives the estimated contributions to the overall single-sideband mixer conversion loss, defined as the ratio (expressed in dB) of the signal power in a free-space Gaussian beam at the mixer input to the output power at the IF frequency. Adding all of these terms together gives a net loss in the range 13.2–15.2 dB. By far the largest contribution (10–12 dB) comes from the intrinsic conversion loss of the junction, which was calculated using Tucker's SIS mixer theory [1] in the 3-port approximation. The large (2 dB) range in the calculated intrinsic conversion loss arises mainly from uncertainties in the capacitance of the junction and to a lesser extent from the uncertainties in the exact impedance of our circuit. It appears that our experimental value of 13 dB for

the *single sideband* conversion loss agrees with at least the lower end of the theoretical range (note that the term "Other optical effects" in Table I should be excluded in this comparison, since these effects do not affect coupling to our hot and cold loads). It should be possible to obtain a large improvement in the coupling efficiency and sensitivity by tuning out the junction capacitance to improve the impedance match. This modification would reduce the intrinsic conversion loss to only a few dB. In addition, the reflection losses could be eliminated by anti-reflection coatings on the lenses.

ACKNOWLEDGMENT

We wish to thank T. Büttgenbach and J. Stern for helpful discussions, J. Carlstrom for assistance with the measurements, and R. Pöpel for communicating the results of his nonlocal calculations of the surface impedance of Nb. J. Z. is indebted to K. Y. Lo and T. G. Phillips for advice and encouragement, and to F. Sharifi and D. Van Harlingen for his introduction to superconducting device fabrication.

REFERENCES

[1] J. R. Tucker and M. J. Feldman, "Quantum detection at millimeter wavelengths," *Rev. Mod. Phys.*, vol. 57, pp. 1055–1113, 1985.
[2] W. C. Danchi and E. C. Sutton, "Frequency dependence of quasiparticle mixers," *J. Appl. Phys.*, vol. 60, pp. 3967–3977, 1986.
[3] M. J. Wengler and D. P. Woody, "Quantum noise in heterodyne detection," *IEEE J. Quantum Electron.*, vol. QE-23, pp. 613–622, 1987.
[4] M. Wengler, D. P. Woody, R. E. Miller, and T. G. Phillips, "A low noise receiver for millimeter and submillimeter wavelengths," *Int. J. Infrared and Millimeter Waves*, vol. 6, pp. 697–706, 1985.
[5] T. H. Büttgenbach, R. E. Miller, M. J. Wengler, D. M. Watson, and T. G. Phillips, "A broad-band low-noise SIS receiver for submillimeter astronomy," *IEEE Trans. Microwave Theory Tech.*, vol. MTT-36, pp. 1720–1726, Dec. 1988.
[6] X. Li, P. L. Richards, and F. L. Lloyd, "SIS quasiparticle mixers with bow-tie antennas," *Int'l J. IR and MM Waves*, vol. 9, pp. 101–133, 1988.
[7] B. N. Ellison, P. L. Schaffer, W. Schaal, D. Vail, and R. E. Miller, "A 345 GHz SIS receiver for radio astronomy," *Int'l J. IR and MM Waves*, vol. 10, pp. 937–947, 1989.
[8] A. R. Kerr, P. H. Siegel, and R. J. Mattauch, "A simple quasi-optical mixer for 100–120 GHz," in *1977 IEEE MTT-S Int. Microwave Symp. Dig.*, 1977, p. 96.
[9] J. G. Heston, J. M. Lewis, S. M. Wentworth, and D. P. Neikirk, "Twin slot antenna structures integrated with microbolometer detectors for 94 GHz imaging," *Micr. Opt. Tech. Lett.*, vol. 4, pp. 15–19, 1991.
[10] M. Kominami, D. M. Pozar, and D. H. Schaubert, "Dipole and slot elements and arrays on semi-infinite substrates," *IEEE Trans. Antennas Propagat.*, vol. AP-33, pp. 600–607, 1985.
[11] E. E. Russell and E. E. Bell, "Measurement of the optical constants of crystal quartz in the far infrared with the asymmetric Fourier-transform method," *J. Opt. Soc. Am.*, vol. 57, pp. 341–348, 1967.
[12] E. V. Loewenstein, D. R. Smith, and R. L. Morgan, "Optical constants of far infrared materials 2: crystalline solids," *Appl. Opt.*, vol. 12, pp. 398–406, 1973.
[13] C. R. Brewitt-Taylor, D. J. Gunton, and H. D. Rees, "Planar antennas on a dielectric surface," *Electron. Lett.*, vol. 17, pp. 729–731, 1981.
[14] M. Born and E. Wolf, *Principles of Optics*, 6th edition, ch. 5. Oxford: Pergamon Press, 1987.
[15] J. F. Whitaker, R. Sobolewski, D. R. Dykaar, T. Y. Hsiang, and G. A. Mourou, "Propagation model for ultrafast signals on superconducting dispersive striplines," *IEEE Trans. Microwave Theory Tech.*, vol. 36, pp. 277–285, 1988.
[16] R. L. Kautz, "Picosecond pulses on superconducting striplines," *J. Appl. Phys.*, vol. 49, pp. 308–314, 1978.
[17] E. Hammerstad and O. Jensen, "Accurate models for microstrip computer-aided design," in *IEEE MTT-S Int. Microwave Symp. Dig.*, 1980, pp. 407–409.
[18] D. C. Mattis and J. Bardeen, "Theory of the anomalous skin effect in normal and superconducting metals," *Phys. Rev.*, vol. 111, pp. 412–417, 1958.
[19] R. Pöpel, "Electromagnetic properties of superconductors," in *Superconducting Quantum Electronics*, V. Kose, Ed., Berlin: Springer, 1989, pp. 44–47.
[20] R. Pöpel, private communication, 1991.
[21] D. P. McGinnis and J. B. Beyer, "A broad-band microwave superconducting thin-film transformer," *IEEE Trans. Microwave Theory Tech.*, vol. 36, pp. 1521–1525, 1988.
[22] B. A. Syrett, "A broad-band element for microstrip bias or tuning circuits," *IEEE Trans. Microwave Theory Tech.*, vol. MTT-28, pp. 925–927, 1980.
[23] J. Stern, private communication, 1991.
[24] V. P. Koshelets, S. A. Kovtonyuk, I. L. Serpuchenko, L. V. Filipenko, and A. V. Shchukin, "High quality Nb-AlO_x-Nb junctions for microwave receivers and SFQ logic device," *IEEE Trans. Magn.*, vol. MAG-27, pp. 3141–3144, 1991.
[25] A. W. Lichtenberger, C. P. McClay, R. J. Mattauch, and M. J. Feldman, "Fabrication of Nb/Al-Al_2O_3/Nb junctions with extremely low leakage currents," *IEEE Trans. Magn.*, vol. MAG-25, 1247–1250, 1989.
[26] H. G. LeDuc, J. A. Stern, S. Thakoor, and S. Khanna, "All refractory NbN/MbO/NbN SIS tunnel junctions," *IEEE Trans. Magn.*, vol. MAG-23, pp. 863–865, 1987.
[27] Norland Optical Adhesive #61, Norland Products Inc., New Brunswick, NJ, or Loctite Litetak, Newington, CT.
[28] L. R. D'Addario, "Saturation of the SIS mixer by out-of-band signals," *IEEE Trans. Microwave Theory Tech.*, vol. 36, pp. 1103–1105, 1988.
[29] Infrared Laboratories, Inc., Tucson, AZ.
[30] Berkshire Technologies, Inc., Oakland, CA.
[31] J. E. Carlstrom Co., Pasadena, CA.
[32] Radiometer Physics, Bergerwiesenstraße 15, 5309 Meckenheim, F.R.G.
[33] D. P. Woody, R. E. Miller, and M. J. Wengler, "85–115 GHz receivers for radio astronomy," *IEEE Trans. Microwave Theory Tech.*, vol. MTT-33, pp. 90–95, 1985.
[34] T. Büttgenbach, private communication, 1991.
[35] M. J. Feldman, "Theoretical considerations for THz SIS mixers," *Int'l J. IR and MM Waves*, vol. 8, no. 10, pp. 1287–1292, 1987.
[36] D. Winkler and T. Claeson, "High-frequency limits of superconducting tunnel junction mixers," *J. Appl. Phys.*, vol. 62, pp. 4482–4498, 1987.

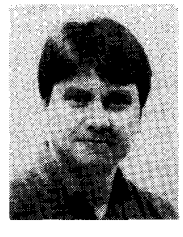

Jonas Zmuidzinas (M'91) was born in Duarte, CA, on September 8, 1960. He received the B.S. degree in physics from the California Institute of Technology in 1981, and the Ph.D. in physics from the University of California, Berkeley in 1987. His Ph.D. thesis described the development of a laser heterodyne receiver for airborne astronomy in the far-infrared (800–2000 GHz).

During 1988–89 he was a postdoctoral fellow at the University of Illinois, where he worked on the design and fabrication of SIS mixers. He is currently an Assistant Professor of Physics at the California Institute of Technology. His research interests are in the areas of high-frequency superconducting devices and their application to submillimeter astronomy.

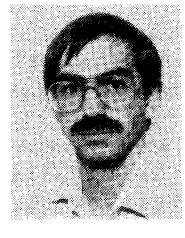

Henry G. LeDuc was born in Butte, MT, on March 8, 1955. He received a B.S. in physics from Montana State University, Bozeman, MT in 1977, and a Ph.D. in physics from the University of California, Davis in 1983. His thesis work involved far-infrared spectroscopy of solid state ionic conductors.

At present, he is a group leader at California Institute of Technology's Jet Propulsion Laboratory. His group is developing SIS tunnel junctions for heterodyne receivers.